

Highlighting nanoparticle aggregation using the time contrast algorithm

D. CHICEA^{a,b}

^aPhysics Dept., University Lucian Blaga of Sibiu, Dr. Ion Ratiu Str. 7-9, Sibiu, 550012, Romania

^bPediatric Respiratory Medicine Research Center (CCMRP), University Lucian Blaga of Sibiu, Romania

The time contrast algorithm proposed in this paper uses a time series recorded in a coherent light scattering experiment performed on a Fe₃O₄ nanofluid during its rapid aggregation in diluted aqueous solution. The time series was analyzed both using the alternative Dynamic Light Scattering data processing algorithm as reference and the time contrast procedure. The time contrast parameter variation is compared with the average aggregates diameter variation during nanoparticles aggregation and the results suggest a simple procedure for qualitative monitoring of the nanoparticles aggregation process.

(Received October 20, 2016; accepted April 6, 2017)

Keywords: Fe₃O₄ nanoparticles, aggregation, DLS, Time contrast.

1. Introduction

Materials exhibit certain physical properties, which are significantly different from their bulk properties when the size of the physical system is reduced to nanometer scale, as quantum effects make themselves manifest [1].

The big surface to volume ratio and their new properties make nanoparticles proper for a wide range of applications starting from building “bricks” for composite materials [2], [3], magnetic devices, pharmaceuticals, sensors, coatings and paints, [4], catalysts [5] and for medical applications [6].

As the nanoparticles size is smaller not only than the cells but than the cell organelles, nanostructured materials have been considered for investigating living cells or for delivering substances or drugs to them. More applications of nanostructured materials in medicine and biology have been imagined and some of them even developed and are presented in review papers, like [7] and [8] to mention just few of them. Nevertheless, in spite of the generalized enthusiasm regarding the nanoparticles promising applications, several warnings on the danger of big amounts of nanoparticles uncontrolled spread in environment were issued [9].

Fe₃O₄ nanoparticles are outstandingly interesting for biomedical applications as they can be metabolized by the living organism and have low toxicity. Reference [10] reports on using a superconducting magnetometer and on detecting ferromagnetic material presence in human brain tissues.

The nanoparticles aggregate very fast when diluted in aqueous carrier fluid [11], [12], [13]. The former nanofluid contains micron sized particles suspended, after aggregation. The nanofluid rheological properties strongly depend of the nanoparticles size distribution and concentration. The body fluids are aqueous solutions, therefore it is of interest for biomedical applications to

have good knowledge of the time scale of the aggregation process.

Several techniques have been used in the study of aggregation process, [14], [15], [16] being just some articles that describe extensively such techniques. Microscopic methods were among the first particle sizing methods that were used [14] followed by sensing zone methods, electrical or optical.

Optical techniques are suited and convenient in monitoring nanoparticle aggregation. Light scattering procedures enable quantitative size analysis [14], [15]. Some of the light scattering procedures that can be used in particle aggregation monitoring are turbidity-wavelength spectra, turbidity fluctuations, small angle light scattering, fractal dimensions of aggregates, Electro-optical effects, sedimentation, filtration, ultrasonic methods [14].

If a coherent light beam is incident on a suspension, the image changes in time and presents fluctuations. These fluctuations are the consequence of the complex motion of sedimentation and of the Brownian (random) motion of the scattering centers (SC hereafter) [13], [14], [15]. Dynamic Light Scattering (DLS), also named Photon Correlation Spectroscopy (PCS), is an optical method that analyzes the correlation of the speckle dynamics with the Brownian motion [17-19].

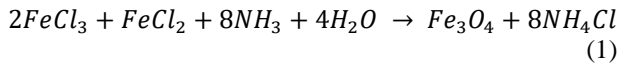
A small amount of Fe₃O₄ nanofluid was synthesized using a coprecipitation method previously described [20], for the work presented here. A brief description is presented in this article together with the results of the nanoparticles characterization.

Dilution experiments with aggregation monitoring were carried on and the results are compared with previous work already reported. Aggregates size was estimated using a modified version of DLS. A new, simple method was tested for a qualitative monitoring of the aggregation process and the results are presented in detail and compared with the DLS results.

2. Materials and methods

2.1. Sample preparation and characterization

A coprecipitation procedure was used to prepare the Fe_3O_4 nanoparticles. The substances used in preparing the sample used in this work were $\text{FeCl}_2 \cdot 4\text{H}_2\text{O}$, $\text{FeCl}_3 \cdot 6\text{H}_2\text{O}$, $\text{NH}_3[\text{aq}]$ (ammonium hydroxide), $\text{C}_6\text{H}_8\text{O}_7$ (citric acid), produced by Merck. Double deionised water was used to dissolve the reagents. The chemical reaction was [12], [20]:



References [21] and [22] highlight that the temperature selected for nanoparticle synthesis deeply changes the size distribution and the chemical composition. Reference [10] states that the temperature range of 65-75 °C will produce spherical magnetite nanoparticles. For this reason the temperature was maintained to 75 °C. More details on nanoparticle synthesis procedure are presented in [13] and [20].

The volume fraction φ of nanoparticle phase in the concentrated nanofluid sample was calculated from mass density measurements using Eq. 2, where ρ_f is the nanofluid density, ρ_l the carrier fluid density and ρ_s the solid particles density. Using Eq. (2) we found that the volume fraction φ of nanoparticles was 8.23%.

$$\varphi = \frac{\rho_f - \rho_l}{\rho_s - \rho_l} \quad (2)$$

The XRD diffraction pattern confirms that the sample is magnetite, Fe_3O_4 . The diffraction pattern is presented in [20] together with details on the experimental conditions used in recording it, therefore is not repeated here. The effective crystallite mean size distribution $D(L)$ for the magnetite sample [20] reveals a wide distribution of the crystallites dimensions with a mean value of 10.9 nm. For nanostructured materials the crystallites dimension equals the mean value of the nanoparticle diameter.

In order to have a size characterization of the nanoparticles using a different physical procedure, a DLS experiment was completed. As pointed out in [11], [12], [13], the aggregation process after aqueous dilution is very fast. For this reason the alternative solvent, 25% citric acid, was used for accurate DLS sizing. The recorded time series was processed using the DLS procedure. The average nanoparticle diameter was found to be 18 nm. This DLS diameter appears to be bigger than the average crystallite size as measured by powder Xray diffraction. The explanation lays in the fact that the DLS provides the hydrodynamic diameter, which is bigger than the physical diameter [12].

2.2. The modified DLS procedure

The experimental setup for DLS is presented in the figure below. It consists of a cuvette containing the sample, a laser source and a detector. A data acquisition system is also necessary, with a computer to record and to process the recording.

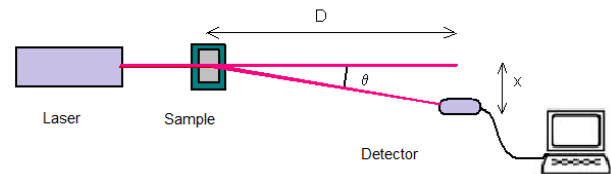


Fig. 1. The DLS experimental setup

D , the distance from the cuvette to the detector, is selected before the experiment in such a manner that the detector size should be approximately equal to the average speckle size. The angle is chosen according to the purpose of the experiment. The angle was smaller for this setup, rather than 90° which is typical for conventional DLS with one detector. More details and reasoning for choosing a smaller angle are presented in [11-13].

Several time series were recorded in this experiment. A sequence of 0.1 s from a time series recorded during the 25-th second of the dilution experiment is presented in Fig. 2. We notice fluctuations of different frequencies.

The recorded electric signal is proportional to the scattered light intensity, therefore the recorded time series is the power time series. The power spectrum is obtained by applying a Fourier transform to the power time series.

The power spectrum of the light intensity scattered by the particles in suspension and the probability density function (hereafter PDF) are not independent [23], [24]. The spectrum derived from the experimental data using the fast Fourier transform can be described using the curve in Eq. (3), which describes the functional form of the Lorentzian line $S(f)$ [12], a function of variable f , the frequency, with two parameters a_0 and a_1 . Using a nonlinear least square minimization and the two parameters that make the best fit of $S(f)$ to the PSD are found.

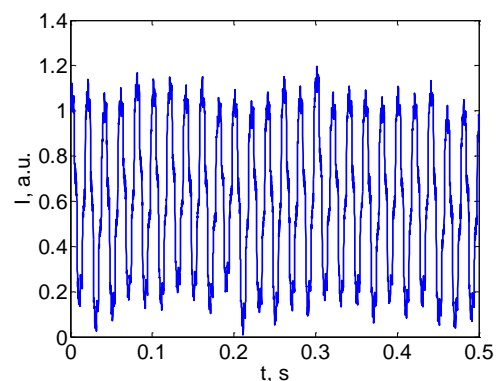


Fig. 2. A sequence of 0.5 s from a time series recorded during the 25-th second of the dilution experiment

$$S(f) = a_0 \cdot \frac{a_1}{(2\pi f)^2 + a_1^2} \quad (3)$$

Fitting $S(f)$ is more time consuming as compared to the easier method [23], [24], of fitting the autocorrelation function or measuring the width at half maximum of the autocorrelation function, because more data points are considered, producing more accurate results.

Once a_0 and a_1 are determined, the diameter of the SCs can be assessed by doubling the radius R calculated using Eq. (4).

$$R = \frac{2k_B T K^2}{6\pi\eta a_1} \quad \text{where} \quad K = \frac{4\pi n}{\lambda} \cdot \sin\left(\frac{\theta}{2}\right) \quad (4)$$

In Eq. (4) k_B is Boltzman's constant, T is the absolute temperature of the sample, η is the dynamic viscosity of the solvent, n is the refractive index of the fluid, θ is the scattering angle and λ is the wavelength of the laser radiation in vacuum [11], [12]. a_0 parameter performs a scaling of the function while a_1 parameter determines the turnover point in a logarithmic scale and is related to the average diameter. More details on the data processing procedure are presented in previous published work [11], [12], [13], where the power spectrum density and the fitted Lorentzian are presented, as well.

The wavelength of the laser beam was 635 nm. The temperature of the suspension was 20 °C. D was 0.46 m and x was 0.040 m, making the scattering angle θ to be 4° 58' 11". The data acquisition rate was 12 kHz. The recording started and the dilution process was initiated by fast injecting a very small amount (0.01 ml) of nanofluid into the cuvette.

2.3. The time contrast procedure

The idea of time contrast is simple and was inspired by the contrast defined in image processing, especially in the Laser Speckle Contrast Imaging (LASCI) [25] that has been used in studying blood flow in tissues for about 30 years and the use has been extended to neuroscience, dermatology and ophthalmology. The technique considers a square area from an image, typical 7x7 pixels, and the spatial contrast is defined as the ratio of the standard deviation of the intensities of each pixel to the mean intensity of that square area. After doing it for all the square areas the image was divided into, another contrast image, with a much smaller resolution (7x7 times smaller) is obtained and the special contrast defined in this manner is related to blood flow rate [22].

TLSCI, which is Time Laser Speckle Contrast Imaging was imagined, as well [26], [27], [28]. TLSCI is used for imaging the time-integrated speckle and produces subsamples with a temporal resolution of 10 Hz. It images all pixels on the image succession in parallel but does not resolve the high frequency temporal variation. It obtains the temporal speckle contrast K_t from the temporal standard deviation of the speckle intensity divided by the average of the intensity. By using temporal sampling to

estimate the speckle contrast, a higher spatial resolution is obtained, at the expense of temporal resolution. More details on these two techniques can be found in [25 -28].

Starting from the above described TLSCI technique, a time contrast algorithm can be imagined on a DLS time series experiment and not on image or image successions processing. Rather than extracting a time series for one particular pixel from consecutive images, the recorded time series in a DLS experiment, is processed.

A recorded time series is actually a collection of values, I_j , $j=1,2, \dots, n$. First the minimum of the whole set is subtracted, producing a new collection that does not contain information related to the static light scattering of the SCs.

The program considers subsets of values from this vector, each subset lasting for the intended time interval. For each subset the standard deviation σ is computed together with the average of the values after subtraction. We define the time contrast K as in Eq. (5):

$$K = \frac{\sigma}{\langle I \rangle} \quad (5)$$

3. Results and discussion

3.1. DLS aggregation monitoring results

A time series was recorded using the parameters describes in subsection 2.2. The time series was split into slices of data, each lasting for 2 s. This time length was chosen to achieve both a good fit (on a reasonable number of experimental data) and a good time resolution of monitoring the aggregate size. More details are presented in previous work published on this subject [12] and [13]. The fitting procedure was carried on in batch mode for all the time slices and the average diameter during that time interval was calculated. Fig. 3 illustrates the variation of the average diameter as time passed.

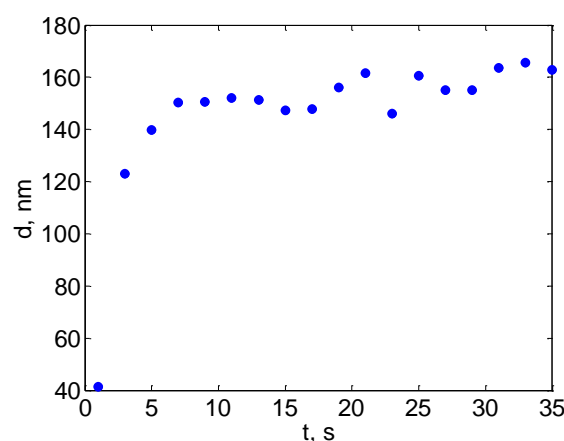


Fig. 3. The variation of aggregates average diameter.

Fig. 3 reveals a rapid increase of the average aggregate diameter. Fig. 3 also reveals that after 4 seconds since dilution was initiated the average measured diameter was bigger than 120 nm. During the following seconds the

average diameter kept increasing but with a slower rate and a plateau can be noticed after 10 seconds from the beginning of the dilution. Fig. 3 also reveals that the aggregate size, assumed to be the diameter, remained around 150 nm and the plateau exhibits a very small slope indicating a further aggregate diameter increase, with a reduced increasing rate though. The fluctuation noticed after 9 seconds can be attributed to the inevitable errors of the fitting procedure [12].

3.2. Time contrast aggregation monitoring results

The same time series that was recorded during the DLS dilution experiment was processed. The time interval for slicing the time series was selected to be 2 s, the same as for the modified DLS processing of the time series. For each slice of the time series the time contrast defined in Eq. (5) was computed.

Fig. 4 illustrates the variation of the time contrast with time passed. Fig. 4 presents a remarkable resemblance with Fig. 3. At the beginning the time contrast K increases rapidly. During the first seconds the value of K kept increasing and a relative plateau can be noticed after 10 seconds from dilution initiation. The values of the time contrast remained around 0.55 and the plateau exhibits a very small slope indicating a further increase, slower though.

The resemblance, strong or weak, of Figs. 3 and 4 naturally raises the question whether there does exist a physical explanation for this feature or it is just a match by chance. A possible explanation can be found in [26] where experimental work with controlled sinusoidal motion of diffusing plates was carried on. The speckle patterns were analyzed using spatio-temporal correlation and “temporal history speckle pattern” [29].

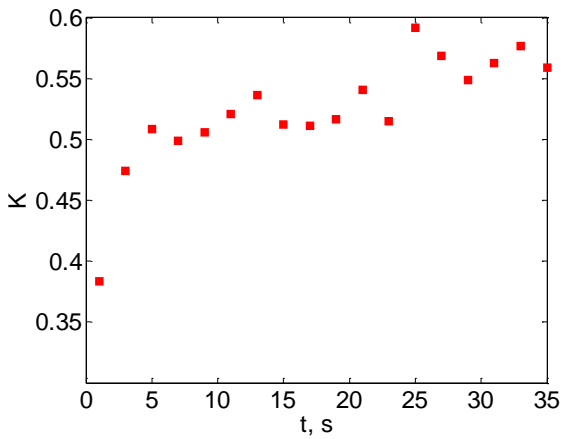


Fig. 4. The variation of the time contrast K during the dilution experiment.

The temporal history speckle pattern on its turn was analyzed using two sub-procedures, the Briers contrast (BC) on time direction [26] and the inertia moment (IM) [30], [31]. During the study both the amplitude and the frequency of the sinusoidal plate motion were modified. The results clearly indicate that the BC is sensitive only to the amplitude of the motion [29]. The BC was reported to increase with the amplitude almost linearly, faster though.

The time contrast definition proposed in this article in Eq. (5) is close to the BC defined in [29], the difference laying in the denominator in (5) which is the average of the recorded intensity rather than the average of the square of the intensity. Moreover, the numerator in the definition used in [29] is the square of the standard deviation while in (5) is the standard deviation. Even so, the definition in Eq. (5) is the ratio of the standard deviation to the average recorded values, with the values made positive by subtracting the minimum of the values in the series and not by squaring [29], therefore the behavior relative to the amplitude dependence will be similar to a certain degree.

For small SCs, with diameter in the nanoscale range, the light scattering can be modeled using the Rayleigh approximation, which states that the light intensity scattered by one particle is proportional to d^6 [32]. During aggregation the volume ratio (nanoparticles/fluid) remains constant as no additional nanofluid is injected. As the SC diameter d increases, the SC number N_n decreases with the diameter d as [12]:

$$N_n = \frac{V_n}{\frac{4\pi}{3} \left(\frac{d}{2}\right)^3} \quad (6)$$

In Eq. (6) V_n is the total volume of the nanoparticles. The average intensity scattered by all the nanoparticles in the laser beam area to a particular direction, as in a DLS experiment, is therefore proportional to d^3 , which results from Eq. (7). Consequently it increases fast with the aggregates diameter [12] and so does the amplitude of the fluctuations.

$$\langle I(\theta) \rangle \sim N_n \cdot d^6; \rightarrow \langle I(\theta) \rangle \sim d^3 \quad (7)$$

This explains why the time contrast K defined as in Eq. (5) is increasing as the aggregation continues and the aggregate diameter increases.

Moving further, we can consider the DLS as a reference method in particle sizing. We can plot the K versus the diameter d assessed by DLS and this plot is illustrated in Fig. 5. Moreover, we can fit a curve to the data in Fig. 5. A good fit with a smooth function on the scattered data in Fig. 5 cannot be made but a reasonable fit was found to be the exponential in Eq. (8), with $R^2 = 0.8561$.

$$K = 0.3281 \cdot e^{0.0032 d} \quad (8)$$

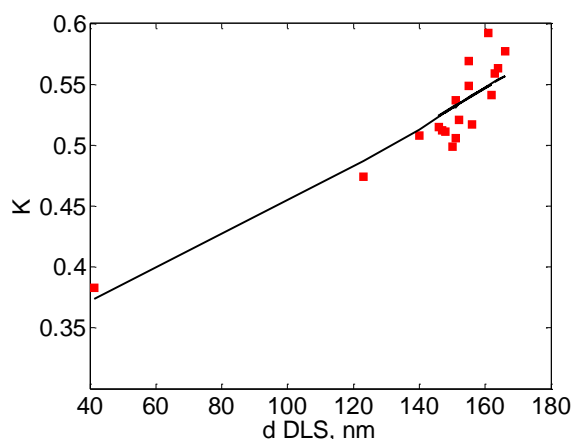


Fig. 5. The pairs d (DLS) – K from the DLS experiment; squares are the experimental data and the continuous line is the exponential fit in Eq. (8)

By reverting Eq. (8) we can find an imprecise, but very simple ansatz for assessing the average diameter of the particles in suspension during the fast aggregation process that carries on in diluted aqueous suspensions, as in Eq. (9), where d is the estimated average diameter, expressed in nm, and K is the time contrast computed for that time slice.

$$d = \frac{1}{0.0032} \cdot \ln \frac{K}{0.3281} \quad (9)$$

4. Conclusion

The time contrast algorithm, defined for a time series recorded during a DLS experiment performed on an aqueous suspension of Fe_3O_4 nanoparticles stabilized with citric acid is presented in detail in this paper. The algorithm has a starting point in the TLSCI and DLS, but presents certain differences though.

First of all, it is not used for imaging. The time series is recorded using a data acquisition system rather than being extracted from a succession of frames in a recording of the speckle field of the coherent light scattered by the growing aggregates from the cuvette. This makes the data acquisition rate, or frequency, much bigger than in TLSCI, where the frame rate dictates the frequency in the time series. A typical frame rate for image recording is 100 to 200 per second, while a 12 kHz acquisition rate was used during the DLS experiment. This makes the time resolution of the time contrast method several hundred times bigger than the LSCI time resolution.

Another difference, from DLS this time, can be found in the data processing algorithm. The DLS involves computing the frequency spectrum using a fast Fourier transform. A function described by Eq. (3), is fit to the power spectrum using a nonlinear minimization procedure producing the hydrodynamical diameter of the particles as an output.

The time contrast involves a much lighter data processing recipe, as compared with the DLS. The time series, whole or a subset, is adjusted by subtracting the average, the standard deviation and the average are computed and, finally, the time contrast is determined. The amount of calculations (in flops) is tremendously smaller and can be performed even on light computing platforms. This makes the procedure much faster on the same computing platform or enables using a light computing platform.

A good resemblance of the trends of the two sets of data points, the variation of the diameter during aggregation, assessed using the alternative DLS data processing algorithm and the time contrast K , defined in the previous section, was found. Several steps are still to be made to have a simple procedure that can be used in measuring the diameter of the scattering centers using the time contrast algorithm. In order to have such a procedure a theoretical model that relates the time contrast to several physical parameters as SC diameter, refractive index of particles and solvent, temperature, wavelength, scattering angle, solvent viscosity, data acquisition rate, to mention just some of them, is still to be improved.

Nevertheless, the very good resemblance of the variation of the average diameter with the time contrast variation is an indication that the time contrast algorithm might be used, at least in a qualitative manner, for monitoring the aggregation process of Fe_3O_4 nanoparticles in diluted aqueous solution.

Acknowledgements

The research presented in this article was in part financed from Lucian Blaga University of Sibiu research grants LBUS-IRG-2016-02.

References

- [1] M. C. Roco, Journal of nanoparticle research **1**(1), 1 (1999).
- [2] V. Rotello, Nanoparticles: Building blocks for nanotechnology, Kluwer Academic/Plenum Publishers, New York, USA, (2004).
- [3] S. Gupta, Q. Zhang, T. Emrick, A. C. Balazs, T. P. Russell, Nature Materials **5**(3), 229 (2006)
- [4] N. A. Kotov, Nanoparticle assemblies and superstructures, Taylor & Francis, Boca Raton, Florida, USA, (2006).
- [5] M. Turner, V. B. Golovko, O. P. Vaughan, P. Abdulkin, A. Berenguer-Murcia, M. S. Tikhov, B. F. Johnson, R. M. Lambert, Nature **454**(7207), 981 (2008).
- [6] X. Gao, Y. Cui, R. M. Levenson, L. W. K. Chung, S. Nie, Nature Biotechnology **22**(8), 969 (2004).
- [7] O. V. Salata, Journal of Nanobiotechnology **2**, 3 (2004).
- [8] V. J. Mohanraj, Y. Chen, Tropical Journal of Pharmaceutical Research **5**(1), 561 (2006).

- [9] G. G. Leppard, *Current Nanoscience* **4**(2), 278 (2008).
- [10] J. L. Kirschvink, A. Kobayashi-Kirschvink, B. J. Woodford, *Proc. Natl. Acad. Sci. U.S.A.* **89**(16), 7683 (1992).
- [11] D. Chicea, *Optoelectron. Adv. Mat.* **4**(9), 1310 (2010).
- [12] D. Chicea, *Current Nanoscience* **8**(6), 259 (2012).
- [13] D. Chicea, *J. Optoelectron. Adv. M.* **15**(9–10), 982 (2013).
- [14] J. Gregory, *Advances in Colloid and Interface Science* **147–148**, 109 (2009).
- [15] R. W. Lines, In *Particle Size Analysis*. Royal Society of Chemistry, Stanley-Wood NG, Lines RW, editors, Cambridge, 350, 1992.
- [16] H. Holthoff, A. Schmitt, A. Fernández-Barbero, M. Borkovec, M. A. Cabrerizo-Vílchez, P. Schurtenberger, R. Hidalgo-Álvarez. *Journal of Colloid and Interface Science* **192**(2), 463 (1997),
- [17] J. W. Goodman, “Laser speckle and related phenomena”, Vol. 9 in series *Topics in Applied Physics*, J.C. Dainty, Ed., Springer-Verlag, Berlin, Heidelberg, New York, Tokyo (1984).
- [18] J. D. Briers, *Laser Doppler, Physiol. Meas.* **22**, R35 (2001).
- [19] M. Giglio, M. Carpineti, A. Vailati, D. Brogioli, *Appl. Opt.* **40**(24), 4036 (2001).
- [20] D. Chicea, E. Indrea, C. M. Cretu, *J. Optoelectron. Adv. M.* **14**(5-6), 46 (2012).
- [21] L. Vayssieres, C. Chaneac, E. Tronc, J. P. Jolinet, *Journal of Colloid and Interface Science* **205**, 205 (1998).
- [22] Z. L. Liu, Y. J. Liu, K. L. Yao, Y. H. Ding, J. Tao, X. Wang, *Journal of Materials Synthesis and Processing* **10**, 83 (2002).
- [23] S. B. Dubin, J. H. Lunacek, G. B. Benedek: *PNAS* **57**(5), 1164 (1967).
- [24] N. A. Clark, J. H. Lunacek, G. B. Benedek, *American Journal of Physics* **38**(5), 575 (1970).
- [25] David A. Boas, Andrew K. Dunn, *J. Biomed. Opt.* **15**(1): 011109_1 (2010).
- [26] P. Li, S. Ni, L. Zhang, S. Zeng, Q. Luo, *Opt. Lett.* **31**, 1824 (2006).
- [27] H. Cheng, Q. Luo, S. Zeng, S. Chen, J. Cen, H. Gong, *J. Biomed. Opt.* **8**, 559 (2003).
- [28] K. R. Forrester, J. Tulip, C. Leonard, C. Stewart, R. C. Bray, *IEEE Trans. Biomed. Eng.* **51**, 2074 (2004).
- [29] R. Nassif, C. A. Nader, F. Pellen, G. Le Brun, M. Abboud, B. Le Jeune, *Applied Optics* **52**(31), 7564 (2013).
- [30] R. Arizaga, M. Trivi, H. Rabal, *Optics & Laser Technology* **31**(2-31), 163 (1999).
- [31] R. A. Braga Junior, B. O. Silva, G. Rabelo, R. M. Costa, A. M. Enes, N. Cap, H. Rabal, R. Arizaga, M. Trivi, G. Horgan, *Optics and Lasers in Engineering* **45**(3), 390 (2007).
- [32] B. H. Zimm, *J. Chem. Phys.* **13**(4), 141 (1945).

*Corresponding author: dan.chicea@ulbsibiu.ro